

# Integrated Network Pharmacology and in vivo Experimental Validation Approach to Explore the Potential Antioxidant Effects of Annao Pingchong Decoction in Intracerebral Hemorrhage Rats

Xuqing Zhou<sup>1,2,\*</sup>, Xu Wang<sup>1,2,\*</sup>, Jiaqi Li<sup>3,\*</sup>, Mengxue Zhang<sup>4</sup>, Yi Yang<sup>1</sup>, Shihui Lei<sup>1</sup>, Ying He<sup>3</sup>, Hua Yang<sup>3</sup>, Desheng Zhou<sup>4</sup>, Chun Guo<sup>1,2</sup>

<sup>1</sup>Experiment Center of Medical Innovation, the First Hospital of Hunan University of Chinese Medicine, Changsha, Hunan, 410007, People's Republic of China; <sup>2</sup>The First Clinical College of Traditional Chinese Medicine, Hunan University of Chinese Medicine, Changsha, Hunan, 410007, People's Republic of China; <sup>3</sup>College of Bioscience and Biotechnology, Hunan Agricultural University, Changsha, Hunan, 410128, People's Republic of China; <sup>4</sup>Department of Neurology, the First Hospital of Hunan University of Chinese Medicine, Changsha, Hunan, 410007, People's Republic of China

\*These authors contributed equally to this work

Correspondence: Chun Guo, Email chunguom@163.com

**Background:** Annao Pingchong decoction (ANPCD) is a traditional Chinese decoction which has definite effects on treating intracerebral hemorrhage (ICH) validated through clinical and experimental studies. However, the impact of ANPCD on oxidative stress (OS) after ICH remains unclear and is worth further investigating.

**Aim:** To investigate whether the therapeutic effects of ANPCD on ICH are related to alleviating OS damage and seek potential targets for its antioxidant effects.

**Materials and Methods:** The therapeutic candidate genes of ANPCD on ICH were identified through a comparison of the target genes of ANPCD, target genes of ICH and differentially expressed genes (DEGs). Protein–protein interaction (PPI) network analysis and functional enrichment analysis were combined with targets-related literature to select suitable antioxidant targets. The affinity between ANPCD and the selected target was verified using macromolecular docking. Subsequently, the effects of ANPCD on OS and the selected target were further investigated through in vivo experiments.

**Results:** Forty-eight candidate genes were screened, in which silent information regulator sirtuin 1 (SIRT1) is one of the core genes that has antioxidant effects and ICH significantly affected its expression. The good affinity between 6 compounds of ANPCD and SIRT1 was also demonstrated by macromolecular docking. The results of in vivo experiments demonstrated that ANPCD significantly decreased modified neurological severity scoring (mNSS) scores and serum MDA and 8-OHdG content in ICH rats, while significantly increasing serum SOD and CAT activity, complicated with the up-regulation of ANPCD on SIRT1, FOXO1, PGC-1 $\alpha$  and Nrf2. Furthermore, ANPCD significantly decreased the apoptosis rate and the expression of apoptosis-related proteins (P53, cytochrome c and caspase-3).

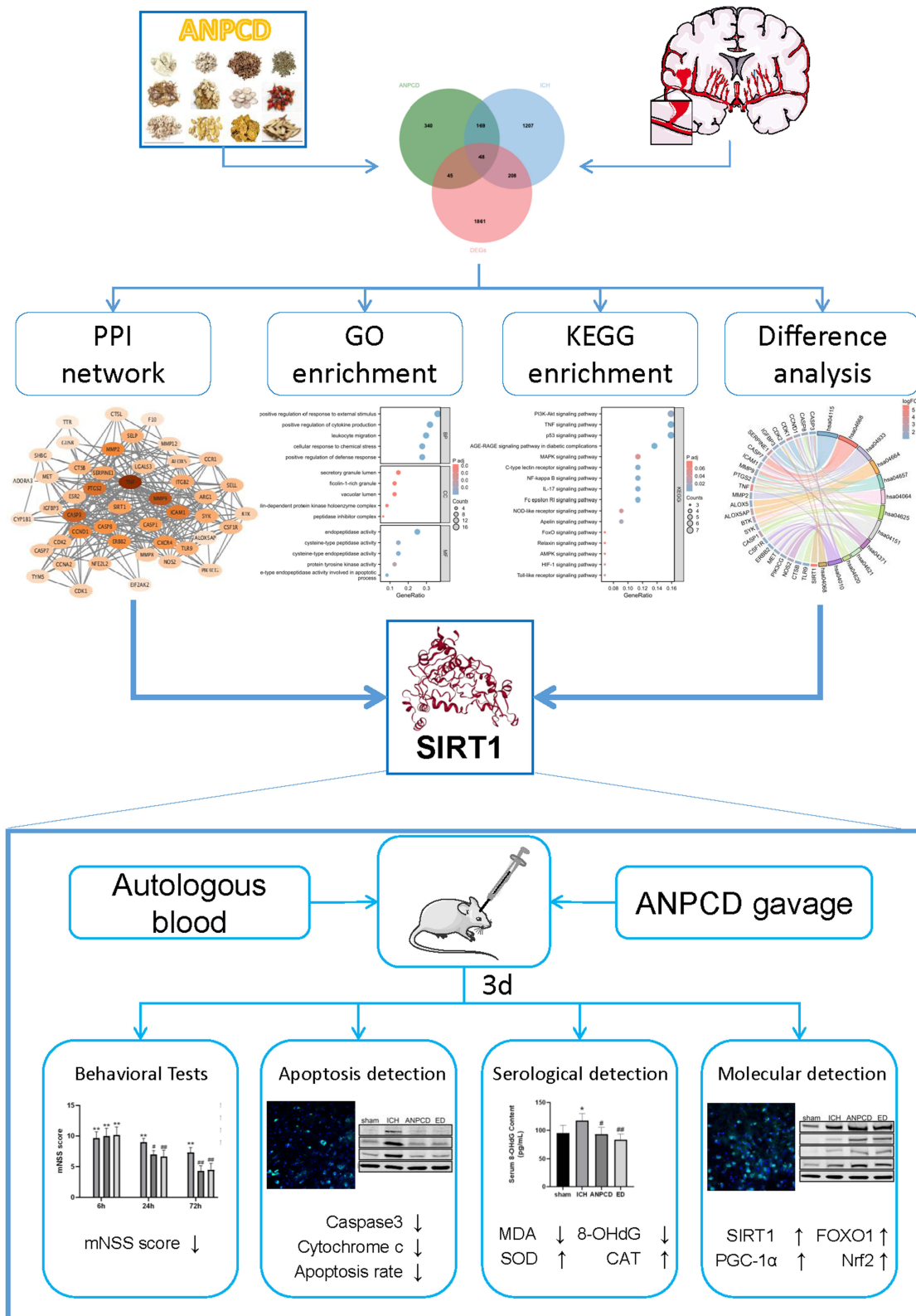
**Conclusion:** ANPCD alleviates OS damage and apoptosis after ICH in rats. As a potential therapeutic target, SIRT1 can be effectively regulated by ANPCD, as are its downstream proteins.

**Keywords:** intracerebral hemorrhage, Annao Pingchong decoction, oxidative stress, network pharmacology, vivo experiments, SIRT1

## Introduction

Intracerebral hemorrhage (ICH) is a cerebrovascular disease that has significantly affected people's lives worldwide due to its high incidence and mortality and poor outcome.<sup>1–3</sup> The complexity of ICH arises from diverse causes and the interaction of multiple pathological mechanisms. Various factors contribute to ICH formation, including hypertension, smooth muscle cell degeneration, cerebral amyloid angiopathy, oral anticoagulant use, vascular malformations, and

Graphical Abstract



hypercholesterolemia.<sup>4</sup> The development of ICH is driven by interconnected pathological mechanisms such as oxidative stress (OS), inflammation, brain edema, and neuronal apoptosis, which progressively exacerbate brain injury.<sup>5,6</sup> Currently, the treatment of ICH predominantly focuses on managing blood pressure, utilizing anticoagulants and surgery to prevent hematoma expansion, and mitigating risk factors to prevent secondary brain injury. However, there is still insufficient evidence that substantiates the significant improvements in mortality and neurological outcomes following ICH with these treatment modalities.<sup>7</sup> Thus, further research is necessary to identify new targets and develop more effective treatment options for ICH.

OS, characterized by excessive accumulation of reactive oxygen species (ROS), plays an important role in aggravating neuronal cell death and neurological dysfunction after ICH.<sup>6</sup> The excessive ROS directly impairs cellular structures and induces cell death through the oxidation of lipids and DNA, which also results in the formation of oxidation products such as malondialdehyde (MDA) and 8-hydroxy-2-deoxyguanosine (8-OHdG).<sup>8</sup> Studies have demonstrated that an elevated level of hydroxyl radicals, a type of ROS, was detected in the brain tissue around the hematoma in ICH rats, concomitant with an increase in apoptotic cells.<sup>9</sup> Edaravone, an oxygen-free radical scavenger, has been shown to effectively reduce the level of 8-OHdG in the brain and ameliorate neurological impairment in ICH rats.<sup>10</sup> Therefore, alleviating OS has the potential to be a therapeutic strategy against ICH.

Annao Pingchong decoction (ANPCD) is developed from Zhengnan Xifeng Decoction, a well-known Traditional Chinese medicine (TCM) prescription clinically used for the treatment of ICH in China. The clinical and *in vivo* experiments have demonstrated the efficacy of ANPCD in alleviating nerve function deficits in patients and reducing neuroinflammation and cerebral edema in ICH rats.<sup>11–16</sup> Modern pharmacological studies have identified 93 compounds in ANPCD, including baicalin, baicalein, wogonin, oroxylin A, geniposide, genipin, crocin, rhein, emodin, rhynchophylline, isorhynchophylline, and hirsutine. These compounds have exhibited neuroprotective effects through their antioxidant activity in various central nervous system diseases.<sup>11,17–24</sup> These studies suggest that ANPCD may exert its therapeutic effects on ICH through antioxidative mechanisms, but the specific mechanisms have not been elucidated. So this study will investigate the effects of ANPCD on OS after ICH to elucidate its neuroprotection.

The synergistic effects of numerous compounds are the key that TCM prescriptions exert comprehensive treatment and regulation across multiple sites and targets, but pose a challenge to the study of their molecular mechanisms. However, network pharmacology (NP) presents a solution by taking TCM prescriptions as a whole to examine the interactions and collective effects among diverse compounds.<sup>25,26</sup> NP integrates network science and computer technology to establish a sophisticated “compound-protein/gene-disease” network, which propels a shift from the conventional “one disease-one target-one drug” medical paradigm to an innovative “network targeted, multi-component treatment” model.<sup>27,28</sup> In this study, we will screen therapeutic targets of ANPCD against ICH through NP, determine the effects of a target on OS by investigating relevant literature, and finally validate the effects of ANPCD on this target and OS via *in vivo* experiments.

## Materials and Methods

### Network Pharmacology Analysis

To screen the therapeutic targets of ANPCD on ICH, we firstly obtained the active components of ANPCD and its corresponding target genes through related references and symmap database (<https://www.symmap.org/>), in which OB (oral bioavailability)  $\geq 30$  and DL (drug-likeness)  $\geq 0.18$  (PMID: 37849727). Then GeneCards database (<https://www.genecards.org/>) was used to screen potential therapeutic target genes for ICH with Relevance Scores of greater than 5 (PMID: 36785707). Meanwhile, a network of disease-herb-active ingredient-target was obtained from symmap database (<https://www.symmap.org/>). Then, active ingredients were further screened based on 48 active plasma components of ANPCD found in a previous study,<sup>11</sup> and targets were further screened based on the filter conditions for Degree  $> 1$ .

### Transcriptome Data Difference Analysis

The data set of ICH-related transcriptome (GSE206971) was screened by searching for the keywords “Intracerebral hemorrhage” and “brain” in the GEO database (<https://www.ncbi.nlm.nih.gov/geo/>). In this data set, the samples of sham

group and ICH group ( $n = 3$ ) were separately obtained. After normalizing the original counts matrix via the VST (Variance Stabilizing Transformations) method, the difference was analyzed according to the standard process by using the DESeq2 package (PMID: 25516281). The screening criteria for differentially expressed genes (DEGs) are following:  $|\log(\text{fold change})| \geq 1$ ,  $p$  value  $< 0.05$ . Then, ggplot2 package (<https://ggplot2.tidyverse.org>) was used to visualize the results. Finally, the overlapping genes between DEGs, targets of ANPCD and targets of ICH were obtained via the jvenn tools (<http://jvenn.toulouse.inra.fr/app/example.html>).

## Protein–Protein Interaction (PPI) Network Analysis

The PPI network analysis of candidate genes was conducted in STRING website (<https://string-db.org/>). Then the nodes and edges of the network were adjusted via the network visualization tool Cytoscape (<https://cytoscape.org>). MCODE plugin (<https://apps.cytoscape.org/apps/mcode>) was used to cluster and score the PPI network and capture the main clusters.

## Functional Enrichment Analysis

After ID conversion of the input molecular list via the R language org.Hs.eg.db package (<https://www.bioconductor.org/packages/release/data/annotation/html/org.Hs.egdb.html>), the GO and KEGG enrichment analysis was conducted by using the clusterProfiler package (<https://bioconductor.org/packages/release/bioc/html/clusterProfiler.htm>), in which the results that  $p$  value  $< 0.05$  were screened. The visualization of the results is achieved by using ggplot2 (<https://ggplot2.tidyverse.org>), igraph packages (<https://igraph.org/>) and ggraph packages (<https://exts.ggplot2.tidyverse.org/ggraph.html>).

## Macromolecular Docking

The PDB data (<https://www.rcsb.org/>) was used to obtain the PDB file of molecular structure of proteins corresponding to the selected target genes, while the SDF file of the active components of ANPCD was obtained via the PubChem database (<https://pubchem.ncbi.nlm.nih.gov/>). Finally, the online molecular docking tool CB-Dock2 (<https://add.labshare.cn/cb-dock2/>) was used for macromolecular docking between target proteins and small-molecule ligands and to calculate its minimum free energy and display the pocket with the minimum free energy.

## Drug Preparation

All herbs of ANPCD were purchased from the Pharmacy Department of the First Hospital of Hunan University of Chinese Medicine, Changsha, Hunan Province, China. The components of ANPCD were shown in [Supplementary Table 1](#), and its preparation was conducted as our previous study mentioned.<sup>11</sup> Edaravone and dexborneol concentrated solution for injection (ED), a clinical drug for alleviating oxidative stress damage in cerebral infarction, was obtained from Simcere Pharmaceutical Co. Ltd. (Nanjing, China).

## Animals and Grouping

All male Sprague–Dawley rats (SD rats) were obtained from Hunan Slac Jingda Laboratory Animal Co., Ltd., Changsha, China (license No. SCXK (Xiang) 2019–0004)). They were housed in a regular and clean room with a temperature of  $24 \pm 2$  °C, relative humidity of 50–70% and 12 h alternate light–dark cycles and had free access to water and food. After a one-week acclimation period, rats weighing between 280 and 320 g were randomly divided into four groups ( $n = 6$ ): sham group, ICH model group, ANPCD treatment group (7.5 g/kg, gavage) and ED treatment group (5.4 mg/kg, intraperitoneal injection). The study was in accordance with the US guidelines (NIH publication #85-23, revised in 1985) for laboratory animal use and care and approved by the Ethics Committee for Experimental Animals of the First Hospital of the Hunan University of Chinese Medicine (Approval No.: ZYFY20220222-7).

## Intracerebral Hemorrhage Model

According to a previous study,<sup>11</sup> 80  $\mu\text{L}$  autologous whole blood drawn by cardiac was injected at a uniform speed into the left caudate nucleus, which was positioned 3 mm lateral to the midline, 1 mm posterior to the bregma, and 6 mm ventral to the skull's surface. After 10 minutes of injection, the needle was slowly withdrawn approximately 2 mm and kept in place for 4 minutes before being completely removed. Then the wound was sutured and disinfected and rats were

returned to separate cages and allowed to recover. The sham group were processed with same procedure without autologous blood injection.

## Drug Administrations

The rats were administered for the first time within 2 h of ICH induction and then gavaged twice or intraperitoneally injected once daily. Rats of ANPCD treatment group take 7.5 g/kg of ANPCD by gavage every day, which was calculated by conversion corresponding to the clinical dose and has been proven to have therapeutic effects,<sup>11</sup> while sham and ICH model group administered equal volume of saline. Meanwhile, it is known according to the drug instructions that the ratio of edaravone and dexborneol is 4:1 and adults can take 60 mg of edaravone intravenously every day. Based on the human-to-rat body mass ratio (the human body weight was set at 70 kg), 5.4 mg/kg of edaravone and 1.35 mg/kg of dexborneol were calculated by conversion and intraperitoneally injected every day. At 72 h, the rats were sacrificed to collect abdominal aorta blood and brain tissue.

## Neurological Deficit Score

To evaluate the neurological deficit of rats, the modified neurological severity score (mNSS) was used respectively at 6, 24 and 72 h after ICH induction, including motor, sensory and beam balance tests, reflexes absent and abnormal movements. It ranged from 0 to 18, in which the higher score was associated with more serious neurological deficit (shown in [Supplementary Table 2](#)).

## ELISA Assay

Rat 8-OHdG enzyme-linked immunosorbent assay (ELISA) kit (ADS-R00208A) was obtained from Jiangsu Aidisheng Biotechnology Co., Ltd (Jiangsu, China). After standing for 1 h, the collected abdominal aorta blood was centrifuged for 10 min at 3500 rpm/min and then supernate was collected and stored at  $-80^{\circ}\text{C}$  until use. Diluted serum sample (10ul serum samples + 40ul sample diluent) was added to the sample wells, while 50ul standard was added to the standard wells, in which the standard with a concentration of 0 was considered as blank control. Except for blank well, 100ul of HRP-conjugate reagent was added to each well and incubated for 1 h at  $37^{\circ}\text{C}$ . Then, each well was washed 5 times with wash solution, added 50ul chromogen solution A and 50ul chromogen solution B and incubated in the dark for 15 minutes at  $37^{\circ}\text{C}$ . Next, 50ul stop solution was added to each well to terminate the reaction. Finally, an automatic microplate reader (Enspire, PerkinElmer, USA) was used to detect the optical density (OD) of each well at 450 nm.

## Measurements of CAT Activity, SOD Activity and MDA Content

CAT assay kit (micro-method) (BC0205) and MDA assay kit (micro-method) (BC0025) were purchased from Beijing Solarbio Science & Technology Co., Ltd (Beijing, China), while SOD assay kit (WST-1 method) (A001-3) was obtained from Nanjing Jiancheng Bioengineering Institute (Nanjing, China). After operating following the instructions, the date of results was collected and analyzed.

## Tissue Treatment

After collecting abdominal aorta blood, the brain tissue around hematoma was collected from 3 rats in each group for WB experiment, while the whole brain tissue of the other 3 rats was used to prepare frozen sections. Briefly, the brains were perfused transcardially with 0.9% sodium chloride solution followed by 4% paraformaldehyde. The entire brains were then carefully removed and immersed in 4% paraformaldehyde for 24 hours. Subsequently, the brains were dehydrated by sequentially immersing them in 15%, 30%, and 35% sucrose solutions for 24 hours at each concentration. After embedding the brain tissue, cryo embedding medium (BL557A, Biosharp, China) solidified rapidly by cooling in a low-temperature environment. Finally, frozen sections of 20  $\mu\text{m}$  thickness in the coronal plane were cut using a freezing microtome (3050S, Leica, Germany).

## TUNEL Staining

The TUNEL apoptosis detection kit (MK1027) was obtained from Wuhan Boster Biological Technology Co., Ltd (Wuhan, China). Firstly, brain tissue frozen sections were washed twice for 2 min each in 0.01 M PBS and the same operation was subsequently implemented in distilled water. Then sections were treated with diluted Proteinase K (1:200) for 60s and washed 3 times for 2 min each in 0.01 M TBS. Labeling Buffer with Terminal deoxynucleotidyl Transferase (TdT) and Digoxin labeled dUTP (DIG-dUTP) was used to label the sections for 2 h at 37°C. After washing 3 times for 2 min each in 0.01 M TBS, the sections were blocked with blocking solution for 30 min at room temperature and incubated with Anti-DIG-Biotin and streptoenzyme avidin-fluorescein FITC (SABC-FITC) respectively for 30 min at 37°C. Finally, the sections were washed 4 times for 5 min each to remove excess reagents and the slices were sealed with antifade mounting media with DAPI (S2110, Solarbio, China). Under a laser confocal microscope (LSM800, Zeiss, Germany), TUNEL-positive cells identified by green fluorescence of FITC were counted. The apoptosis ratio = TUNEL-positive cells/total cell number  $\times$  100%.

## Immunofluorescence Staining

After washing twice for 10 min each in 0.01 M PBS, brain tissue frozen sections were blocked with 3% bovine serum albumin for 30 min. The primary antibodies were added and incubated overnight at 4 °C. Then the sections were washed thrice in PBS for 15 min each and incubated with a secondary antibody in the dark for 1 h at 20–25 °C. After sealing with antifade mounting media with DAPI (S2110, Solarbio, China), the slices were observed under a laser confocal microscope (LSM800, Zeiss, Germany). The primary antibodies were following: SIRT1 mouse monoclonal (1:2000, ab110304, Abcam), FOXO1 rabbit polyclonal (1:800, 18592-1-AP, Proteintech), PGC-1 $\alpha$  mouse monoclonal (1:500, 66369-1-Ig, Proteintech) and Nrf2 rabbit polyclonal (1:500, 16396-AP, Proteintech) antibodies.

## Western Blot Analysis

RIPA lysis buffer (BL504A, Biosharp, China) containing protease inhibitors (BL629A, Biosharp, China) was used to lyse and homogenize brain tissue fragments in an ice bath for 30 min. After centrifuging at 12,000 rpm/min at 4°C for 5 min, the supernatant is collected and normalized to a solution with equal protein concentration according to its protein concentration determined by a BCA protein assay kit (BL521A, Biosharp, China). Then the samples were loaded on sodium dodecyl sulfate-polyacrylamide gel electrophoresis (SDS-PAGE) to separate different proteins, which were then electrotransferred to polyvinylidene fluoride (PVDF) membranes (ISEQ00010, Millipore, USA). After blocking with 5% bovine serum albumin for 2 h, the membranes were incubated with the primary antibodies overnight at 4 °C. Next, the membranes were washed 3 times with TBST for 10 min each and incubated with horseradish peroxidase (HRP)-conjugated secondary antibody for 1.5 h at room temperature. After washing 3 times with TBST for 10 min, the blots were visualized by enhanced chemiluminescence (ECL) chemiluminescence assay kits (AR1197, Boster, China) and multicolor fluorescence imaging analysis system (FluorChem R, Proteinsimple, USA). Finally, the relative density of the protein bands was quantified by the Image J software. The primary antibodies are following: SIRT1 rabbit polyclonal (1:1000, 13161-1-AP, Proteintech), FOXO1 rabbit polyclonal (1:1000, 18592-1-AP, Proteintech), PGC-1 $\alpha$  rabbit polyclonal (1:1000, ab72230, Abcam), Nrf2 rabbit polyclonal (1:1000, 16396-AP, Proteintech), P53 rabbit polyclonal (1:1000, 10442-1-AP, Proteintech), cytochrome c rabbit polyclonal (1:1000, 10993-1-AP, Proteintech), Caspase 3 rabbit polyclonal (1:1000, 19677-1-AP, Proteintech) and GAPDH mouse monoclonal (1:5000, YM3029, Immunoway) antibodies.

## Statistical Analysis

All data are presented as mean  $\pm$  standard deviation and analyzed using GraphPad Prism (version 9.0). Data sets were analyzed for comparisons between two groups using *t*-test or multiple comparisons using one-way ANOVA and Tukey's multiple comparison tests. Statistical significance was set at  $P < 0.05$ .

## Results

### Forty-Eight Candidate Genes and 15 Core Genes are Obtained by NP, Transcriptome Data Difference Analysis and PPI Analysis

The TCMSP database has shown that 163 active components in 12 herbs of ANPCD were screened, of which the corresponding relationship network was shown in [supplementary Figure 1](#) and [supplementary Table 3](#). Moreover, 602 related target genes were also obtained from active components of ANPCD according to TCMSP database and 1632 potential therapeutic target genes for ICH were also screened from GeneCards database. Then, the network of disease-herb-active ingredient-target was drawn and shown in [Figure 1](#).

After analyzing the difference between Sham samples (n=3) and ICH samples (n=3) in Transcriptome data set (GSE206971), 2162 differentially expressed genes (DEGs) were screened ([Figure 2A](#)) and then compared with the target

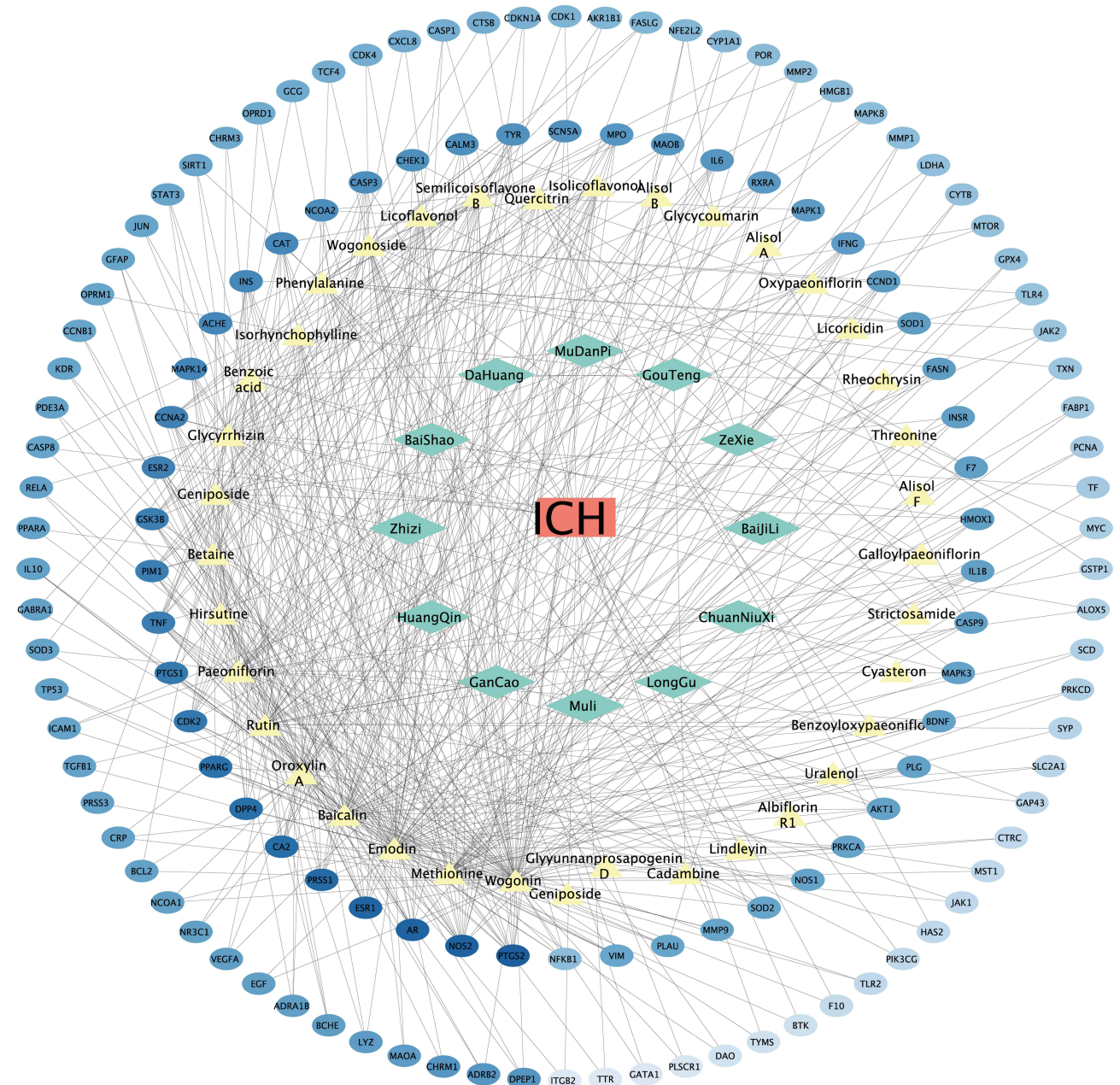


**Figure 1** The network diagram of disease-herb-active ingredient-target. The red rectangle represents disease; the green diamond represents 12 herbs of ANPCD; the yellow triangle represents 48 active plasma components of ANPCD and the blue ellipse represents targets.

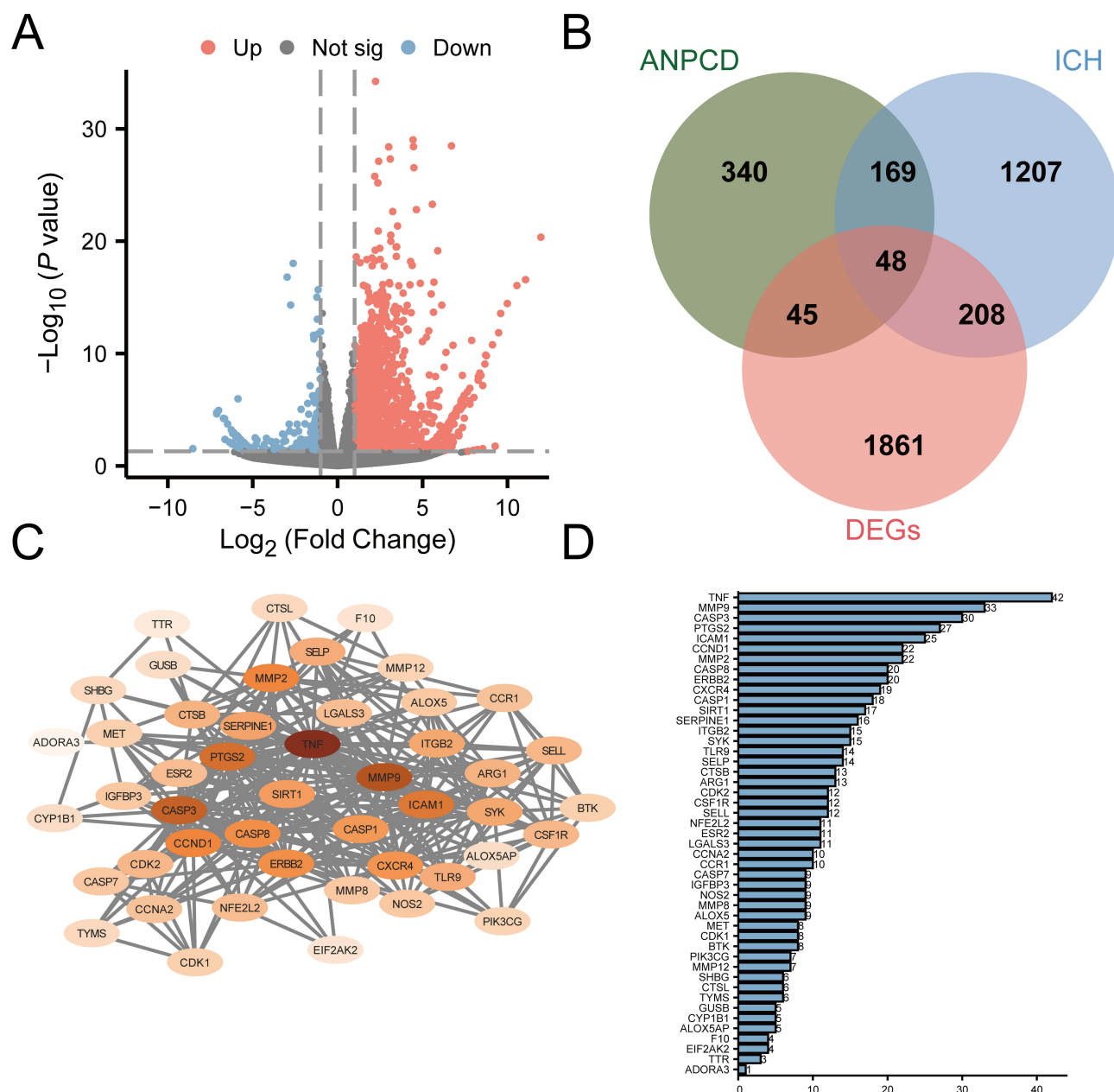


**Figure 2** NP, transcriptome data difference analysis and PPI analysis screened 48 potential therapeutic target genes of ANPCD against ICH. **(A)** Volcano map of differential analysis between sham and ICH in transcriptome data set (GSE206971). **(B)** Venn diagram of overlapping genes between DEGs, targets of ANPCD and targets of ICH. **(C)** The PPI network diagram of 48 candidate genes, in which the darker colors represent higher Degree value. **(D)** Ranking bar chart of Degree value in PPI network graph, in which the horizontal axis represents Degree.

genes of ANPCD and ICH, in which 48 candidate genes were obtained (Figure 2B). Then, PPI network analysis of 48 candidate genes was conducted through the STRING website (Figure 2C) and 15 core genes were obtained according to sorting results of the degree of nodes and edges (Figure 2D).

Based on the results of differential analysis, the heat map of 15 core genes is shown in Figure 3A. Then 15 core genes were divided into three main clusters by modularizing the PPI network via the MCODE plugin to show nodes in each cluster, which was following: Cluster1 contains 11 nodes, in which the core genes are PTGS2, CCND1, and MMP2 (Figure 3B); Cluster2 includes 11 nodes, in which TNF, MMP9 and ICAM1 are the core genes (Figure 3C); Cluster3 consists of 12 nodes that take CASP3, CXCR4, and SIRT1 as the core genes (Figure 3D).

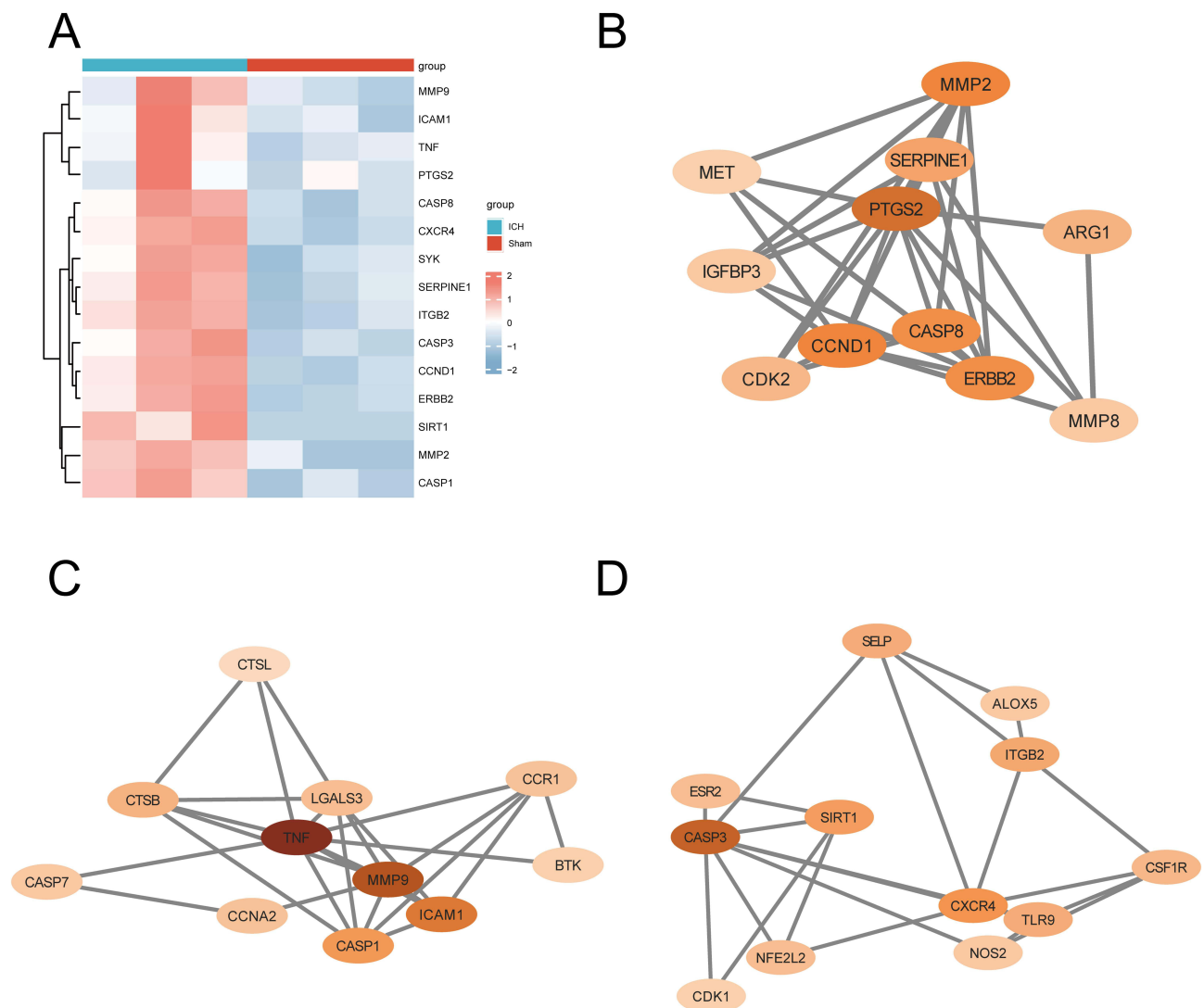


**Figure 3** The cluster analysis of 15 core genes and PPI network diagram of each of cluster: **(A)** Heat map of 15 core genes. **(B)** PPI network diagram of cluster1. **(C)** PPI network diagram of cluster2. **(D)** PPI network diagram of cluster3.

## SIRT1 is Regarded as a Potential Therapeutic Target of ANPCD on ICH

The results of GO enrichment analysis demonstrated that 48 candidate genes participated in multiple biological processes (BP), including positive regulation of response to external stimuli (GO: 0032103), positive regulation of defense response (GO: 0031349), positive regulation of cytokine production (GO: 0001819), leucocyte migration (GO: 0050900) and cellular response to chemical stress (GO: 0062197), and their effects on molecular function (MF) and cellular component (CC) are also shown in [Figure 4A](#). The signaling pathways that candidate genes mainly participate in were screened through KEGG enrichment analysis, consisting of PI3K Akt signaling pathway, TNF signaling pathway, p53 signaling pathway, MAPK signaling pathway, and FoxO signaling pathway ([Figure 4B](#)). After visualized ([Figure 4C](#)), the KEGG analysis results were combined with the results of the  $\log_2$  (Fold Change) values in the difference analysis to draw a chord diagram. It is found that silent information regulator sirtuin 1 (SIRT1), which has high  $\log_2$  (Fold Change) values, mainly participates in the FoxO signaling pathway ([Figure 4D](#), [Table 1](#)).

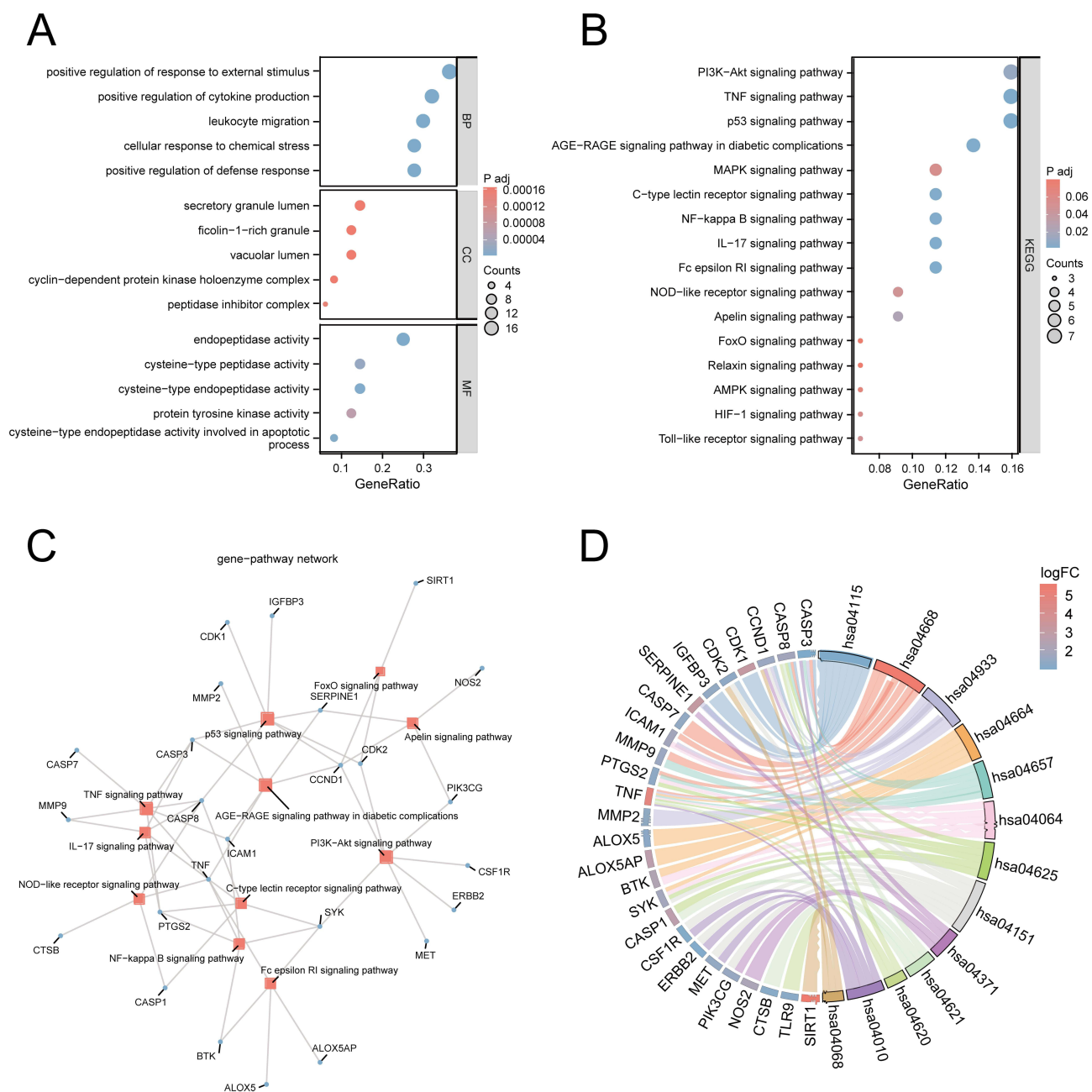


**Figure 4** Functional enrichment analysis of 48 candidate genes. **(A)** GO enrichment analysis of 48 candidate genes in BP, MF and CC. **(B)** KEGG enrichment analysis of 48 candidate genes. **(C)** Gene-pathway network diagram. **(D)** The chord diagram represents the combined results of  $\log_2$  (Fold Change) values, genes and pathways. The left side represents genes, while the right side represents pathways.

## Six Compounds of ANPCD Can Effectively Bind with SIRT1

After obtaining the molecular structure of SIRT1 protein (PDB ID:4ZZJ), we screened 8 active components of ANPCD that may have effects on SIRT1 from the PubChem database. Then, the minimum free energy between these components and SIRT1 was counted through CB-Dock2 (shown in Table 2). The results showed that the minimum free energy between SIRT1 and 6 active components, including phenylalanine, licoricone, rhynchophylline, hirsutine, wogonin and oroxylin A, was less than  $-6$  kcal/mol and these active components could form hydrogen bonds with SIRT1 protein (Figure 5), indicating that these active components had strong binding activity to SIRT1.

**Table 1** The Signaling Pathway Regulated by the Compounds of ANPCD

ID	Description
hsa04115	P53 signaling pathway
hsa04668	TNF signaling pathway
hsa04933	AGE-RAGE signaling pathway in diabetic complications
hsa04664	Fc epsilon RI signaling pathway
hsa04657	IL-17 signaling pathway
hsa04064	NF-kappa B signaling pathway
hsa04625	C-type lectin receptor signaling pathway
hsa04151	PI3K-Akt signaling pathway
hsa04371	Apelin signaling pathway
hsa04621	NOD-like receptor signaling pathway
hsa04620	Toll-like receptor signaling pathway
hsa04010	MAPK signaling pathway
hsa04068	FoxO signaling pathway

**Table 2** Molecular Docking Energy Between 8 Active Compounds of ANPCD and Core Gene-Related Protein SIRT1

Ingredient	Molecular Docking Energy/ (kcal mol <sup>-1</sup> )
Threonine (PubChem CID:6288)	-4.8
Methionine (PubChem CID:6137)	-4.5
Phenylalanine (PubChem CID:6140)	-6.5
Licoricone (PubChem CID:5319013)	-8.5
Rhynchophylline (PubChem CID:5281408)	-10.2
Hirsutine (PubChem CID:3037884)	-8.5
Wogonin (PubChem CID:5281703)	-6.3
Oroxylin A (PubChem CID:5320315)	-8.6

## ANPCD Alleviates ICH-Induced Neurological Deficit in Rats

At 6 h after ICH induction or sham operation, the scores in ICH model group and treatment groups significantly increased compared with sham group. However, ANPCD and ED significantly decreased the scores at 24 h and 72 h, indicating that ANPCD exerts neuroprotective effects by promoting the recovery of neurological function (Figure 6A).

## ANPCD Decreases Serum 8-OHdG and MDA Content and Increases Serum SOD and CAT Activity

To determine whether the antioxidant effects of ANPCD are associated with the recovery of neurological function, we detected separately the activity of superoxide dismutase (SOD) and catalase (CAT) and the content of malondialdehyde (MDA) and 8-hydroxy-2-deoxyguanosine (8-OHdG) in serum of ICH rats at 72 h. Compared with ICH group, ANPCD and ED significantly decreased the content of MDA and 8-OHdG, but increased the activity of SOD and CAT activity (Figure 6B-E).

## ANPCD Increases the Expression of SIRT1, FOXO1, PGC-1 $\alpha$ and Nrf2

To further elucidate the antioxidant mechanism exerted by ANPCD, Western blot and immunofluorescence staining were used to detect the protein expression of SIRT1, forkhead box O transcription factor 1 (FOXO1), peroxisome proliferator-

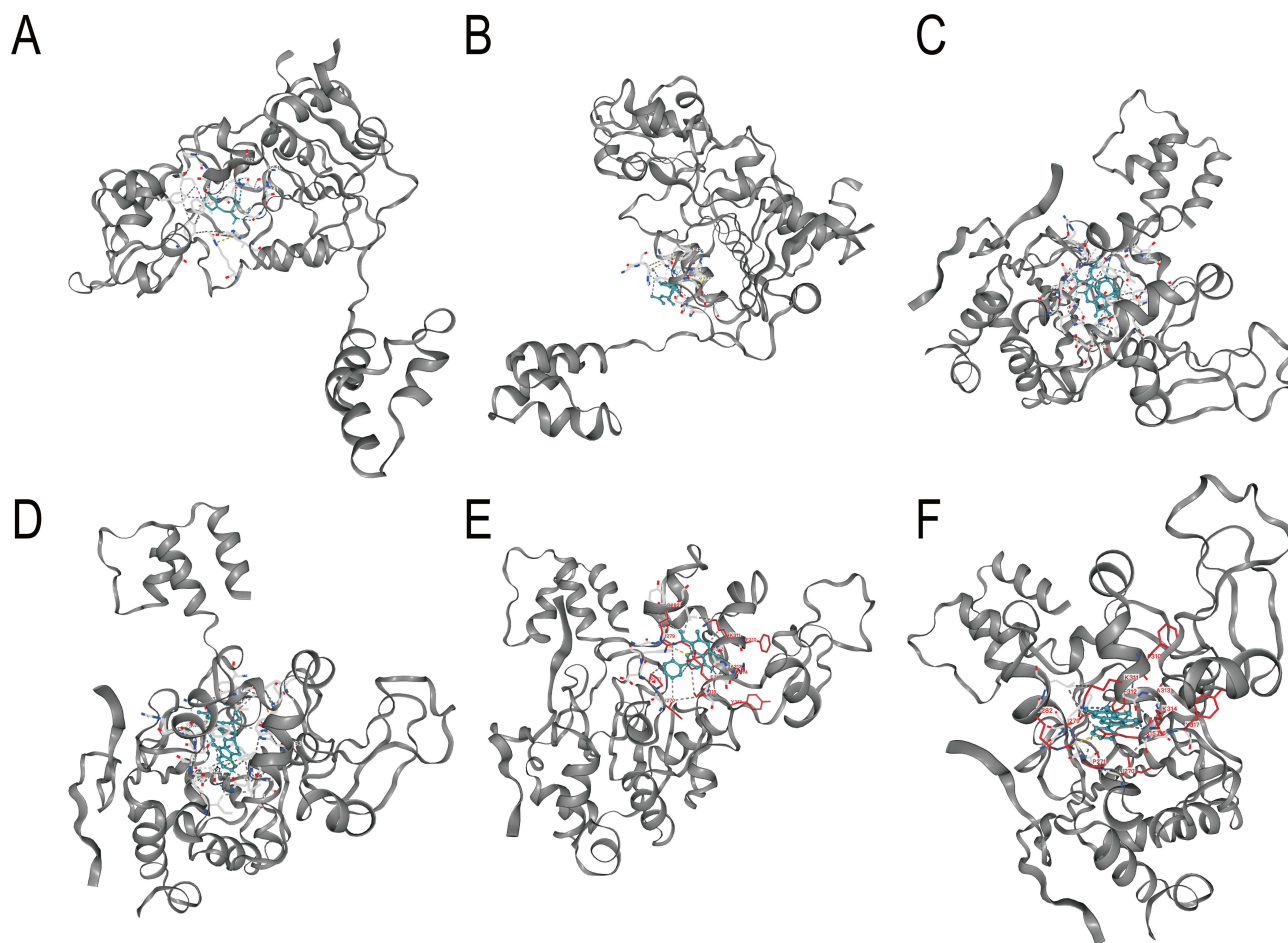


**Figure 5** The macromolecular docking between SIRT1 and six active components that ANPCD. **(A)** macromolecular docking of SIRT1 with Phenylalanine. **(B)** macromolecular docking of SIRT1 with Licorice. **(C)** macromolecular docking of SIRT1 with Rhynchophylline. **(D)** macromolecular docking of SIRT1 with Hirsutine. **(E)** macromolecular docking of SIRT1 with Wogonin. **(F)** macromolecular docking of SIRT1 with Oroxylin A.

activated receptor- $\gamma$  coactivator-1 $\alpha$  (PGC-1 $\alpha$ ) and nuclear factor-erythroid-2-related factor 2 (Nrf2) in brain tissue around hematoma at 72 h after ICH. As shown in the results, ANPCD and ED significantly up-regulated the expression of these proteins (Figures 7 and 8).

## ANPCD Decreases the Apoptosis Rate and the Expression of P53, Cytochrome c and Caspase-3

To investigate the effects of ANPCD on the OS-induced apoptosis, we used TUNEL staining and Western blot to detect the apoptosis rate and the expression of P53, cytochrome c and caspase-3. After ICH induction, the apoptosis rate significantly increased and the expression of P53, cytochrome c and caspase-3 was significantly up-regulated, while ANPCD and ED effectively counteracted these effects (Figure 9).

## Discussion

OS not only contributes to the pathological process of ICH but also plays an important role in the neurological outcomes of ICH.<sup>29,30</sup> Following ICH, OS is induced by various factors such as hemolysis, mitochondrial dysfunction, and inflammatory reactions, leading to increased production of ROS.<sup>31</sup> Apart from causing direct damage, OS also exacerbates brain tissue injury by promoting neuroinflammation, neural cell death, and disruption of the blood-brain barrier.<sup>6</sup> Clinical Study has also found that a worse outcome for ICH patients was associated with higher MDA levels in the

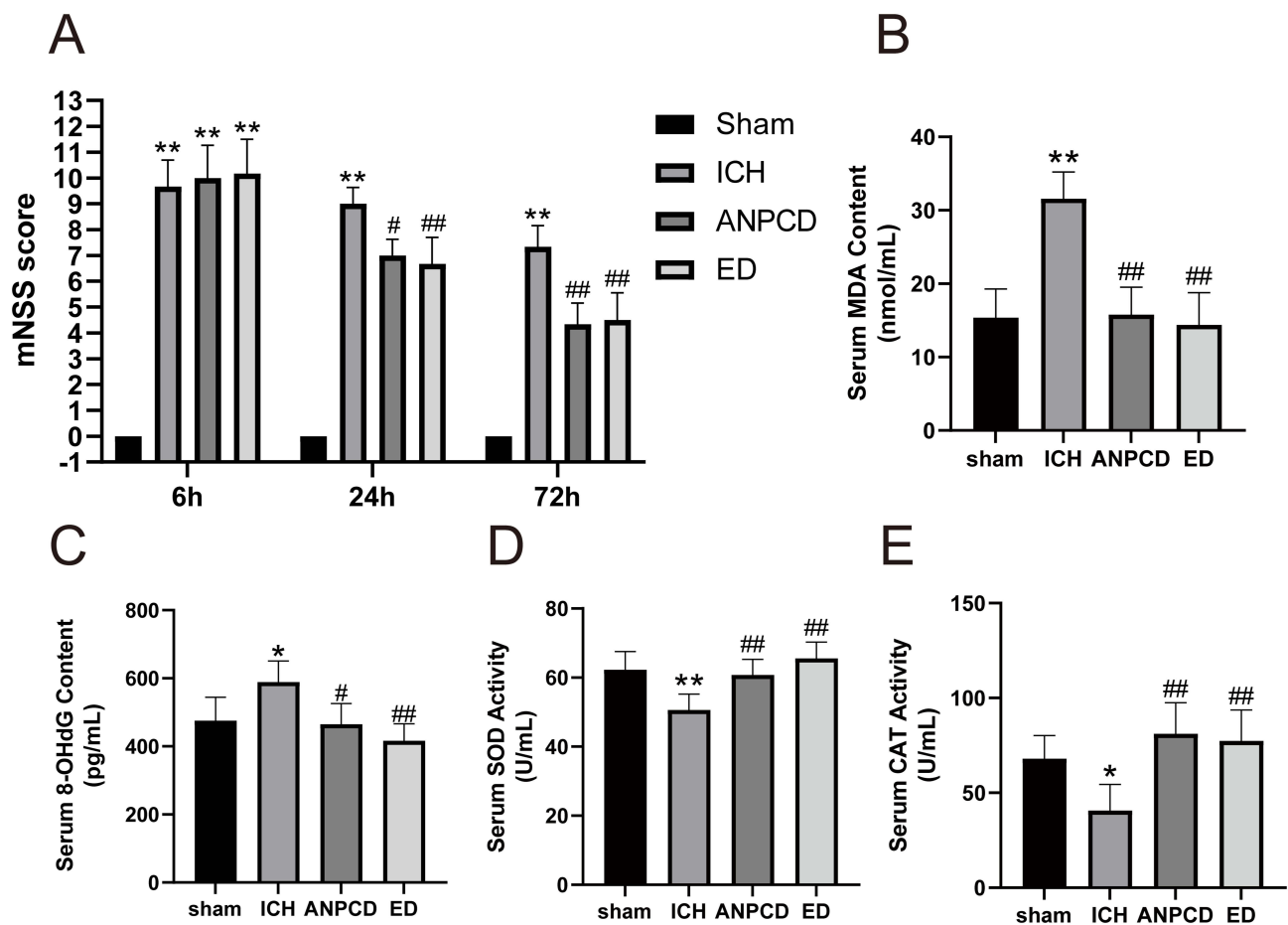


**Figure 6** ANPCD and ED decreased neurological deficit scores and serum MDA and 8-OHdG content, but increased serum SOD and CAT activity at 72 h after ICH in rats. (A) mNSS score. (B) serum MDA content. (C) serum 8-OHdG content. (D) serum SOD activity. (E) serum CAT activity. \*  $p < 0.05$  or \*\*  $p < 0.01$  as compared with the sham group; #  $p < 0.05$  or ##  $p < 0.01$  as compared with the ICH group.

cerebrospinal fluid.<sup>30,32</sup> Hence, exploring treatment methods for reducing OS is essential for developing new and effective drugs for treating ICH.

In China, TCM has extensive researches of the pathomechanisms of ICH and thinks that counterflow ascent of *chong qi* and stirring internally of *wind-fire* is the important one. According to the theory of TCM, all herbs of ANPCD are combined to play therapeutic roles for ICH together, such as settling the liver, extinguishing wind, calming *chong qi*, down-bearing counterflow, and quieting blood and the brain. To further explore the therapeutic mechanism of ANPCD, 15 core genes were screened from 48 therapeutic candidate genes of ANPCD against ICH and the relevant literature was investigated to find out the effects of them on pathological change of ICH. Previous reports have highlighted that SIRT1 protein serves as an NAD<sup>+</sup>-dependent histone deacetylase, playing crucial roles in modulating oxidative stress, inflammatory response, and apoptosis in various disorders of the central nervous system, including Alzheimer's Disease, Parkinson's Disease, Huntington's Disease, and ICH.<sup>33–35</sup> Activating SIRT1 after stroke is considered as an important strategy to inhibit high mobility group protein 1-mediated neuroinflammation to prevent neurodegeneration and ANPCD could exert similar inhibitory effect in our previous study.<sup>11,36</sup> Therefore, based on multiple functions of SIRT1, it is of great significance to study the impact of ANPCD on SIRT1 for clarifying its various pharmacological effects.

Subsequent analysis found that SIRT1 participates in multiple biological processes and has high log<sub>2</sub> (Fold Change) values, indicating that there is a significant difference in the expression of SIRT1 before and after ICH. The strong affinity between SIRT1 and 6 active compounds of ANPCD (phenylalanine, licoricone, rhynchophylline,

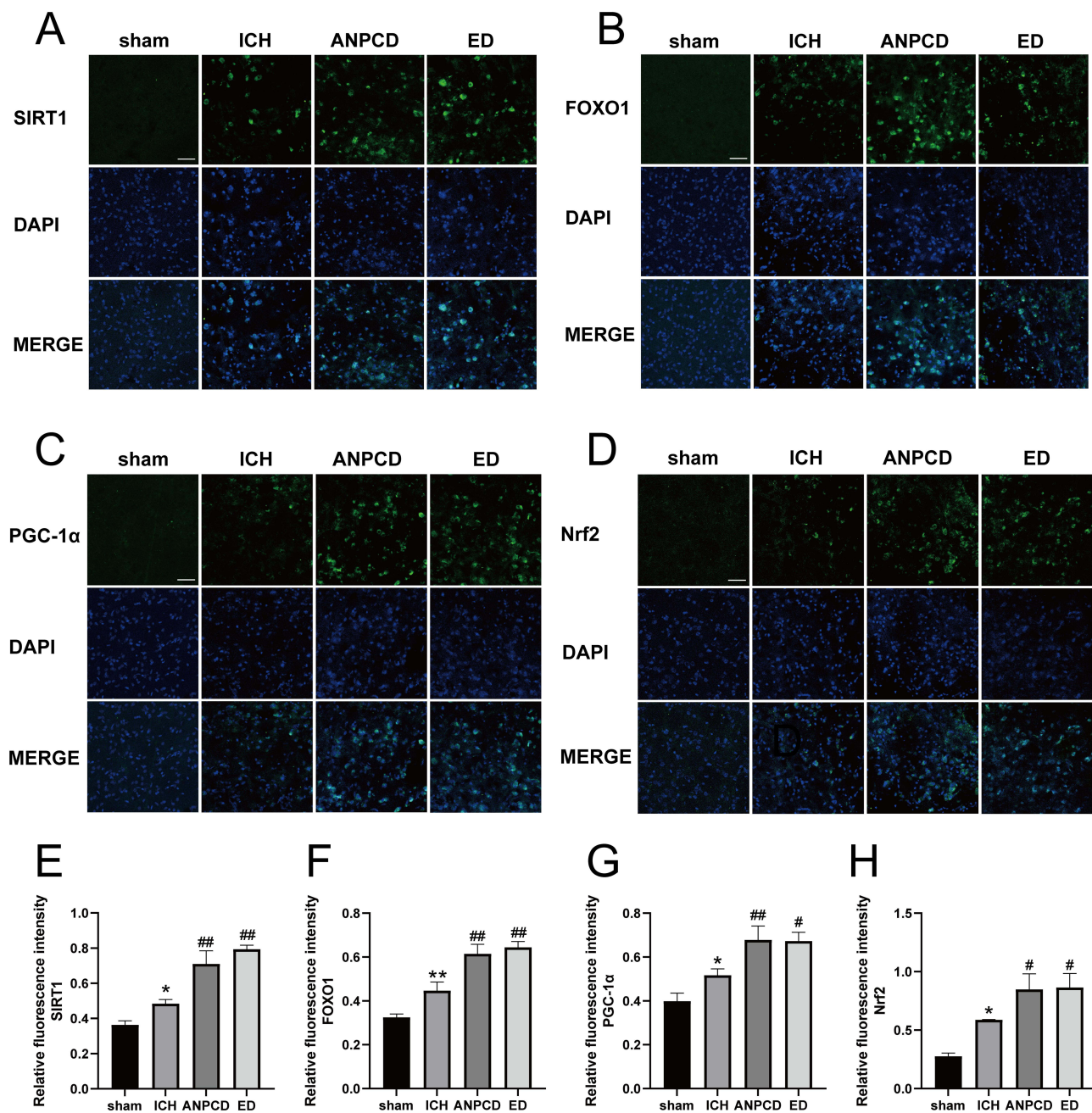


**Figure 7** ANPCD and ED up-regulated the protein expression of SIRT1, FOXO1, PGC-1 $\alpha$  and Nrf2 in brain tissue around hematoma at 72 h after ICH by immunofluorescence staining; Scale bars = 50  $\mu$ m (100  $\times$ ). **(A)** Immunofluorescence of SIRT1 (green) and DAPI (blue). **(B)** Immunofluorescence of FOXO1 (green) and DAPI (blue). **(C)** Immunofluorescence of PGC-1 $\alpha$  (green) and DAPI (blue). **(D)** Immunofluorescence of Nrf2 (green) and DAPI (blue). **(E)** Relative fluorescence intensity of SIRT1. **(F)** Relative fluorescence intensity of FOXO1. **(G)** Relative fluorescence intensity of PGC-1 $\alpha$ . **(H)** Relative fluorescence intensity of Nrf2. \*  $p < 0.05$  or \*\*  $p < 0.01$  as compared with the sham group; #  $p < 0.05$  or ##  $p < 0.01$  as compared with the ICH group.

hirsutine, wogonin and oroxylin A) was further verified through the assessment of minimum free energy. However, whether other compounds of ANPCD regulate SIRT1 requires further research. In view of the antioxidant effects of SIRT1, investigating the regulation of ANPCD on SIRT1 will provide a new insight to comprehend its antioxidant mechanism.

The antioxidant effects of SIRT1 are achieved by regulating the expression and activity of various transcription factors, including FOXO1, PGC-1 $\alpha$  and Nrf2.<sup>37</sup> FOXO1 enhances cellular antioxidant defense by promoting the transcription of antioxidant proteins from different subcellular compartments to respond to ROS and other

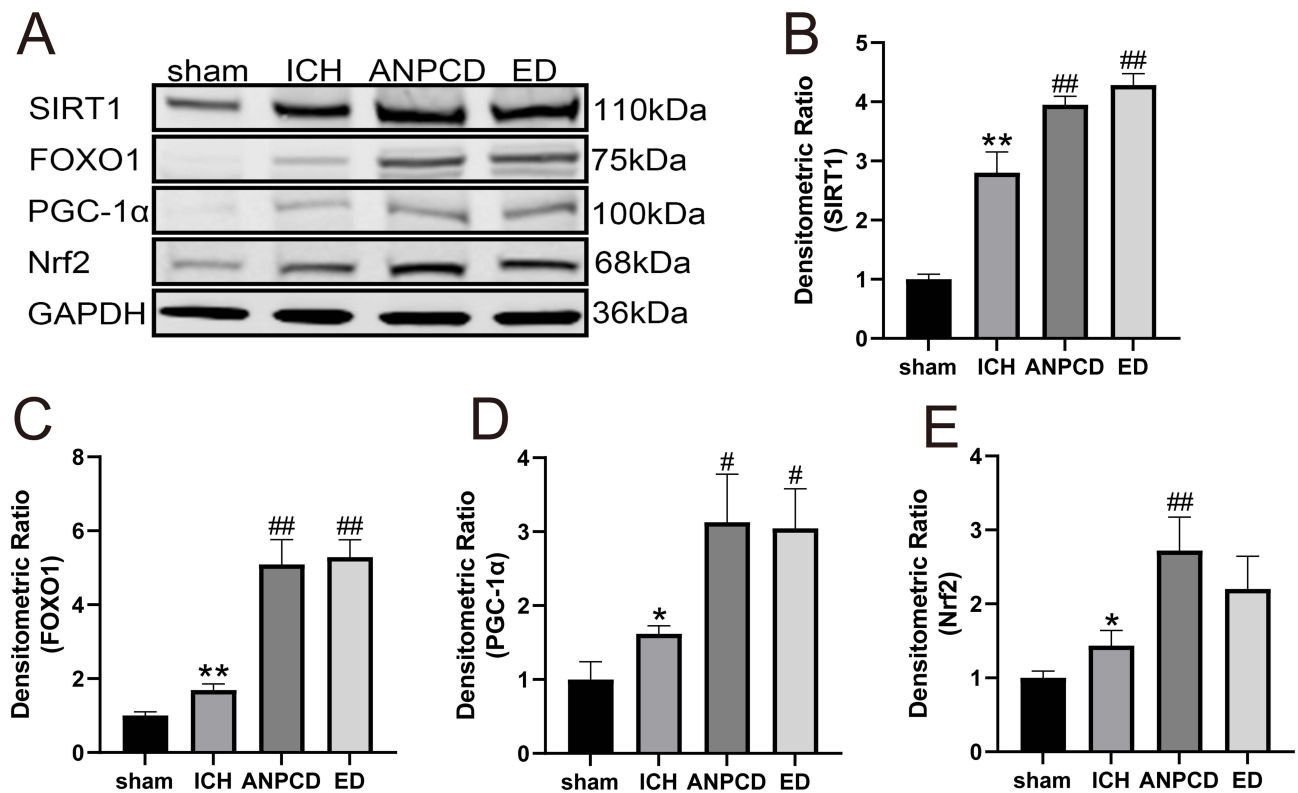


**Figure 8** ANPCD and ED up-regulated the protein expression of SIRT1, FOXO1, PGC-1 $\alpha$  and Nrf2 in brain tissue around hematoma at 72 h after ICH by Western blot. **(A)** The protein expression of SIRT1, FOXO1, PGC-1 $\alpha$  and Nrf2. **(B)** The quantitative densitometric ratio of SIRT1. **(C)** The quantitative densitometric ratio of FOXO1. **(D)** The quantitative densitometric ratio of PGC-1 $\alpha$ . **(E)** The quantitative densitometric ratio of Nrf2. \*  $p < 0.05$  or \*\*  $p < 0.01$  as compared with the sham group; #  $p < 0.05$  or ##  $p < 0.01$  as compared with the ICH group.

stress-inducing stimuli.<sup>38,39</sup> PGC-1 $\alpha$  regulates the expression of multiple mitochondrial antioxidant genes to inhibit the accumulation of ROS, which prevents mitochondrial dysfunction and oxidative injury.<sup>40</sup> Nrf2 protects nerve cells against oxidative injury via the activation of the antioxidant response element (ARE) in neurodegenerative and cerebrovascular diseases.<sup>41</sup> Upon being deacetylated by SIRT1, these transcription factors are activated and interact with antioxidant genes to up-regulate the expression of various antioxidant enzymes, such as SOD and CAT.<sup>39,40,42,43</sup> Furthermore, these transcription factors can directly or indirectly positively regulate each other's activity and expression.<sup>37,38,44</sup> The results of this study showed that ANPCD significantly increased the protein expression of SIRT1, PGC-1 $\alpha$ , FOXO1 and Nrf2, which may be one of the antioxidant mechanisms of ANPCD.

Antioxidative enzyme, including SOD and CAT, is an important defense mechanism that alleviate ROS-induced OS and promotes cell survival by scavenging ROS generated continually during cellular metabolism.<sup>45</sup> During cellular metabolism, the electron transport chain in mitochondria transfers electrons to oxygen, leading to the production of superoxide anion, which is one of the primary ROS.<sup>46</sup> SOD catalyzes the conversion of superoxide anion to hydrogen peroxide, and CAT further catalyzes the breakdown of hydrogen peroxide into water and oxygen.<sup>47</sup> Following ICH, high levels of ROS are rapidly generated, and the antioxidative enzymes can not scavenge them in a timely manner. This leads to an accumulation of oxidation products and exacerbates brain injury.<sup>31</sup> Therefore, increasing the activity of antioxidative enzymes can alleviate OS by scavenging ROS after ICH. In this study, ANPCD significantly decreased neurological deficit scores and serum MDA and 8-OHdG content in ICH rats, which may be related to the fact that it significantly increased activity of SOD and CAT.

Apoptosis is a cell death type which can be induced by OS and plays an important role in the poor prognosis of ICH patients.<sup>48</sup> It is reported that SIRT1 can regulate the activity of P53 to play a key role in a range of cellular events, such as apoptosis.<sup>49</sup> P53 is a vital transcriptional protein that enhances the expression of

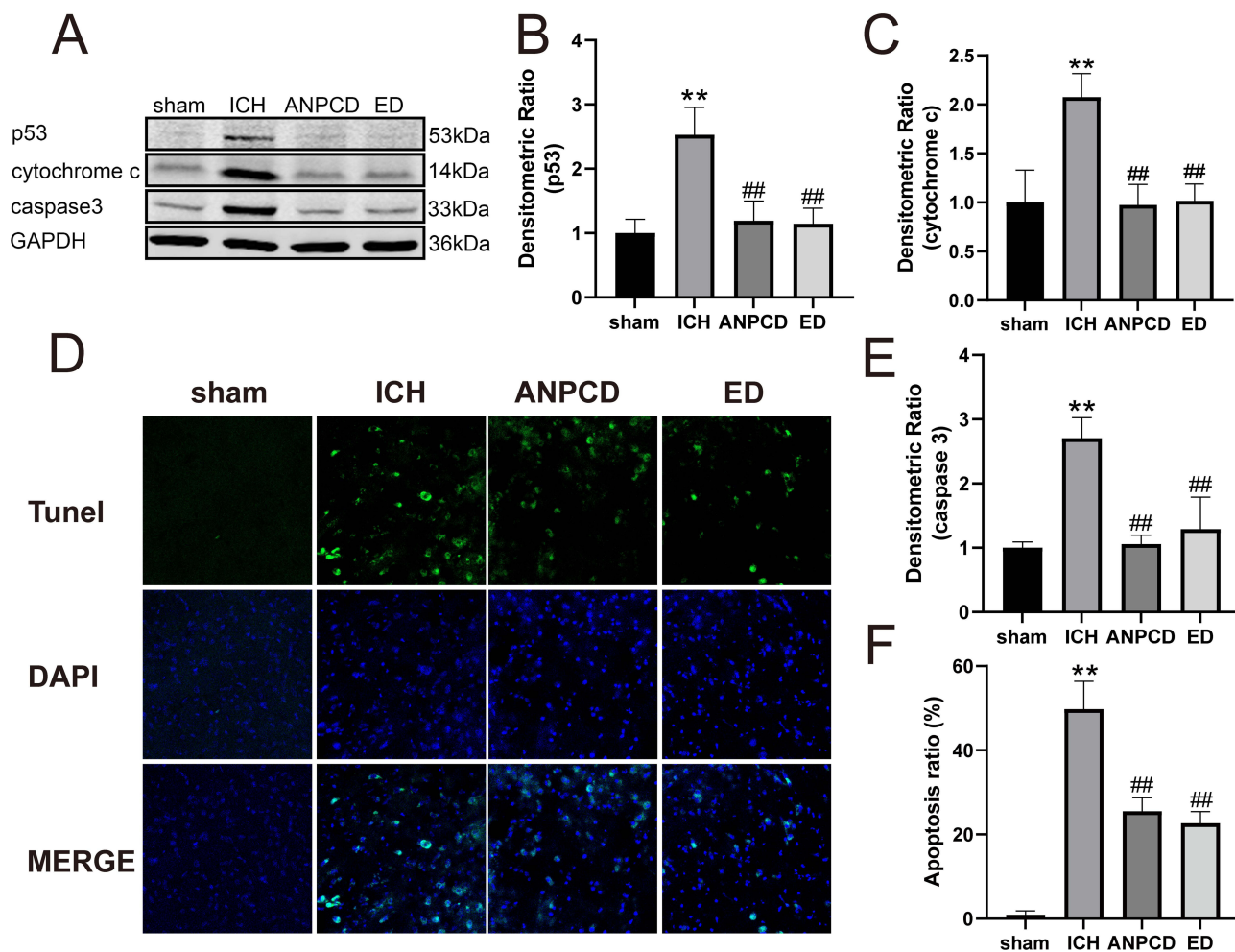


**Figure 9** ANPCD and ED decreases the apoptosis rate and the expression of P53, cytochrome c and caspase-3. **(A)** The protein expression of P53, cytochrome c and caspase-3. **(B)** The quantitative densitometric ratio of P53. **(C)** The quantitative densitometric ratio of cytochrome c. **(D)** TUNEL staining with fluorescence of brain tissue at 72 h after ICH. **(E)** The quantitative densitometric ratio of caspase-3. **(F)** Apoptosis rate. \*\*  $p < 0.01$  as compared with the sham group; ##  $p < 0.01$  as compared with the ICH group.

proapoptotic proteins and triggers the opening of the mitochondrial permeability transition pore (mPTP).<sup>50</sup> Subsequently, cytochrome c is released from the mitochondria through the open mPTP, activating caspases to initiate the cellular apoptosis process.<sup>51</sup> However, the activity of P53 is inhibited after being deacetylated by SIRT1.<sup>52</sup> It has also been demonstrated in experimental subarachnoid hemorrhage rats that an activator of SIRT1 reduced the expression of P53 and neuronal apoptosis.<sup>53</sup> Additionally, this study revealed that ANPCD significantly reduced the apoptosis rate, which could be associated with the down-regulation of P53, cytochrome c, and caspase-3 expression levels.

Our investigation mainly focused on the impact of ANPCD on OS via the regulation of SIRT1 and its downstream proteins. However, the deacetylation effect of SIRT1 on its downstream proteins was not elucidated in detail and worthy of further study. Meanwhile, as one of downstream proteins of SIRT1, PGC-1 $\alpha$  serves as the key regulator of mitochondrial biogenesis.<sup>54</sup> Based on the regulation effect of ANPCD on PGC-1 $\alpha$ , studying alterations in mitochondrial morphology and function might provide more valuable insights into the antioxidative mechanisms of ANPCD. Moreover, although our study identified 48 therapeutic candidate genes and 15 core genes of ANPCD against ICH, the specific involvement of the other 47 genes in the post-ICH pathological processes and the regulatory roles of ANPCD on these genes remain unknown. Therefore, conducting further investigations to

elucidate the roles and mechanisms of ANPCD would greatly contribute to the development of novel and effective drugs for ICH treatment.

## Conclusion

In summary, this study has successfully identified 48 therapeutic candidate genes of ANPCD against ICH and determined that SIRT1 is a potential therapeutic target and has good affinity for ANPCD. Subsequent *in vivo* experiments also confirmed that ANPCD could up-regulate the protein expression of SIRT1, which leads to the further regulation of antioxidase-related transcription factors (FOXO1, PGC-1 $\alpha$ , and Nrf2) and apoptosis-related proteins. These findings shed light on some underlying mechanisms behind the antioxidant and anti-apoptotic effects of ANPCD.

## Abbreviation

ANPCD, Annao Pingchong decoction; CAT, catalase; DEGs, differentially expressed genes; FOXO1, forkhead box O transcription factor 1; ICH, intracerebral hemorrhage; MDA, malondialdehyde; mPTP, mitochondrial permeability transition pore; NP, network pharmacology; Nrf2, nuclear factor-erythroid-2-related factor 2; OS, oxidative stress; PGC-1 $\alpha$ , peroxisome proliferator-activated receptor- $\gamma$  coactivator-1 $\alpha$ ; PPI, protein-protein interaction networks; ROS, reactive oxygen species; SIRT1, silent information regulator sirtuin 1; SOD, superoxide dismutase; TCM, traditional Chinese medicine; 8-OHdG, 8-hydroxy-2-deoxyguanosine.

## Data Sharing Statement

The original contributions presented in this study are included in the article/[Supplementary Material](#), and further inquiries can be directed to the corresponding authors.

## Ethics Statement

The animal study was reviewed and approved by the Ethics Committee for Experimental Animals of the First Hospital of Hunan University of Chinese Medicine.

## Acknowledgments

We thank the Experimental Center of Medical Innovation of The First Hospital of Hunan University of Chinese Medicine for providing the experimental conditions.

## Author Contributions

All authors made a significant contribution to the work reported, whether that is in the conception, study design, execution, acquisition of data, analysis and interpretation, or in all these areas; took part in drafting, revising or critically reviewing the article; gave final approval of the version to be published; have agreed on the journal to which the article has been submitted; and agree to be accountable for all aspects of the work.

## Funding

This work was supported by the National Natural Science Foundation of China (Grant no. 81874463), Natural Science Foundation of Hunan Province (Grant no. 2019JJ50466), the Research Foundation of Health Commission of Hunan Province (Grant no. 20233472), Natural Science Foundation of Changsha (Grant no. Kq2208208), and the Department of Agriculture and Rural Affairs of Hunan Province Research Project (Grant no.2130111).

## Disclosure

The authors declare that the research was conducted in the absence of any commercial or financial relationships that could be construed as potential conflicts of interest.

## References

1. Feigin VL, Krishnamurthi RV, Parmar P, et al. Update on the Global Burden of Ischemic and Hemorrhagic Stroke in 1990-2013: the GBD 2013 Study. *Neuroepidemiology*. 2015;45(3):161–176. doi:10.1159/000441085
2. Poon MT, Fonville AF, Al-Shahi Salman R. Long-term prognosis after intracerebral haemorrhage: systematic review and meta-analysis. *J Neurol Neurosurg Psychiatry*. 2014;85(6):660–667. doi:10.1136/jnnp-2013-306476
3. van Asch CJ, Luitse MJ, Rinkel GJ, van der Tweel I, Algra A, Klijn CJ. Incidence, case fatality, and functional outcome of intracerebral haemorrhage over time, according to age, sex, and ethnic origin: a systematic review and meta-analysis. *Lancet Neurol*. 2010;9(2):167–176. doi:10.1016/S1474-4422(09)70340-0
4. Zille M, Farr TD, Keep RF, Römer C, Xi G, Boltze J. Novel targets, treatments, and advanced models for intracerebral haemorrhage. *EBioMedicine*. 2022;76:103880. doi:10.1016/j.ebiom.2022.103880
5. Chen S, Li L, Peng C, et al. Targeting Oxidative Stress and Inflammatory Response for Blood-Brain Barrier Protection in Intracerebral Hemorrhage. *Antioxid Redox Signal*. 2022;37(1–3):115–134. doi:10.1089/ars.2021.0072
6. Zhang Y, Khan S, Liu Y, Wu G, Yong VW, Xue M. Oxidative Stress Following Intracerebral Hemorrhage: from Molecular Mechanisms to Therapeutic Targets. *Front Immunol*. 2022;13:847246. doi:10.3389/fimmu.2022.847246
7. Magid-Bernstein J, Girard R, Polster S, et al. Cerebral Hemorrhage: pathophysiology, Treatment, and Future Directions. *Circ Res*. 2022;130(8):1204–1229. doi:10.1161/CIRCRESAHA.121.319949
8. Yao Z, Bai Q, Wang G. Mechanisms of Oxidative Stress and Therapeutic Targets following Intracerebral Hemorrhage. *Oxid Med Cell Longev*. 2021;2021:8815441. doi:10.1155/2021/8815441
9. Han N, Ding SJ, Wu T, Zhu YL. Correlation of free radical level and apoptosis after intracerebral hemorrhage in rats. *Neurosci Bull*. 2008;24(6):351–358. doi:10.1007/s12264-008-0711-4
10. Nakamura T, Kuroda Y, Yamashita S, et al. Edevone attenuates brain edema and neurologic deficits in a rat model of acute intracerebral hemorrhage. *Stroke*. 2008;39(2):463–469. doi:10.1161/STROKEAHA.107.486654
11. Guo C, Zhou X, Wang X, et al. Anao Pingchong decoction alleviate the neurological impairment by attenuating neuroinflammation and apoptosis in intracerebral hemorrhage rats. *J Ethnopharmacol*. 2023;310:116298. doi:10.1016/j.jep.2023.116298
12. Zhou D, Chen Y, Li X, et al. Effect of Anao Pingchong Pills on the expression of AQP-9 of peripheral tissue in rats after intracerebral hemorrhage. *J Hunan Univ CM*. 2013;33(05):30–33+55.
13. Guo C, Zhou X, Wang X. Effect of Anao pingchongtang on cerebral edema and the expression of MMP-2/9 after intracerebral hemorrhage. *Chin J Diffic Compl Cas*. 2011;10(02):129–131.
14. Zhou D, Chen Y, Hu H, et al. Influence of Anao pingchong Tang on cerebral edema and expression of AQP-4 after intracerebral hemorrhage in rat. *Chin J Inf TCM*. 2011;18(01):49–50.
15. Zhou D, Liu Q, Wang Q, Dai F. Clinical observation on the treatment of acute thalamic hemorrhage with combination of traditional Chinese and western medicine. *J TCM Univ Hunan*. 2003;1(4):41–43.
16. Zhou D, Liu Q, Dai F, et al. Clinical effect of Anao Pingchong decoction combined with western medicine on acute stage of thalamic hemorrhage. *Chin J Integrat Med*. 2003;2(7):406–407.
17. Kim DH, Kim S, Jeon SJ, et al. The effects of acute and repeated oroxylin A treatments on Abeta(25-35)-induced memory impairment in mice. *Neuropharmacology*. 2008;55(5):639–647. doi:10.1016/j.neuropharm.2008.05.019
18. Kushida H, Matsumoto T, Ikarashi Y. Properties, Pharmacology, and Pharmacokinetics of Active Indole and Oxindole Alkaloids in Uncaria Hook. *Front Pharmacol*. 2021;12:688670. doi:10.3389/fphar.2021.688670
19. Liang W, Huang X, Chen W. The Effects of Baicalin and Baicalein on Cerebral Ischemia: a Review. *Aging Dis*. 2017;8(6):850–867. doi:10.14336/AD.2017.0829
20. Lv S, Ding Y, Zhao H, Liu S, Zhang J, Wang J. Therapeutic Potential and Effective Components of the Chinese Herb Gardeniae Fructus in the Treatment of Senile Disease. *Aging Dis*. 2018;9(6):1153–1164. doi:10.14336/AD.2018.0112
21. Pan L, Cho KS, Yi I, To CH, Chen DF, Do CW. Baicalein, Baicalin, and Wogonin: protective Effects against Ischemia-Induced Neurodegeneration in the Brain and Retina. *Oxid Med Cell Longev*. 2021;2021:8377362. doi:10.1155/2021/8377362
22. Wang C, Zhang D, Ma H, Liu J. Neuroprotective effects of emodin-8-O-beta-D-glucoside in vivo and in vitro. *Eur J Pharmacol*. 2007;577(1–3):58–63. doi:10.1016/j.ejphar.2007.08.033
23. Yang W, Ip SP, Liu L, Xian YF, Lin ZX. Uncaria rhynchophylla and its Major Constituents on Central Nervous System: a Review on Their Pharmacological Actions. *Curr Vasc Pharmacol*. 2020;18(4):346–357. doi:10.2174/1570161117666190704092841
24. Zhao Q, Wang X, Chen A, et al. Rhein protects against cerebral ischemic-/reperfusion-induced oxidative stress and apoptosis in rats. *Int J Mol Med*. 2018;41(5):2802–2812. doi:10.3892/ijmm.2018.3488
25. Luo TT, Lu Y, Yan SK, Xiao X, Rong XL, Guo J. Network Pharmacology in Research of Chinese Medicine Formula: methodology, Application and Prospective. *Chin J Integr Med*. 2020;26(1):72–80. doi:10.1007/s11655-019-3064-0
26. Zhu T, Wang L, Wang LP, Wan Q. Therapeutic targets of neuroprotection and neurorestoration in ischemic stroke: applications for natural compounds from medicinal herbs. *Biomed Pharmacother*. 2022;148:112719. doi:10.1016/j.biopha.2022.112719
27. Nogales C, Mamdouh ZM, List M, Kiel C, Casas AI, Schmidt H. Network pharmacology: curing causal mechanisms instead of treating symptoms. *Trends Pharmacol Sci*. 2022;43(2):136–150. doi:10.1016/j.tips.2021.11.004
28. Zhang R, Zhu X, Bai H, Ning K. Network Pharmacology Databases for Traditional Chinese Medicine: review and Assessment. *Front Pharmacol*. 2019;10:123. doi:10.3389/fphar.2019.00123
29. Duan X, Wen Z, Shen H, Shen M, Chen G. Intracerebral Hemorrhage, Oxidative Stress, and Antioxidant Therapy. *Oxid Med Cell Longev*. 2016;2016:1203285. doi:10.1155/2016/1203285
30. Masomi-Bornwasser J, Kurz E, Frenz C, et al. The Influence of Oxidative Stress on Neurological Outcomes in Spontaneous Intracerebral Hemorrhage. *Biomolecules*. 2021;11(11):1615. doi:10.3390/biom11111615
31. Shao L, Chen S, Ma L. Secondary Brain Injury by Oxidative Stress After Cerebral Hemorrhage: recent Advances. *Front Cell Neurosci*. 2022;16:853589. doi:10.3389/fncel.2022.853589

32. Lorente L, Martín MM, González-Rivero AF, et al. High Serum DNA and RNA Oxidative Damage in Non-surviving Patients with Spontaneous Intracerebral Hemorrhage. *Neurocrit Care*. 2020;33(1):90–96. doi:10.1007/s12028-019-00864-8
33. Deng HJ, Zhou CH, Huang LT, Wen LB, Zhou ML, Wang CX. Activation of silent information regulator 1 exerts a neuroprotective effect after intracerebral hemorrhage by deacetylating NF- $\kappa$ B/p65. *J Neurochem*. 2021;157(3):574–585. doi:10.1111/jnc.15258
34. Liu H, Xu S, Wang C, et al. The Beneficial Role of Sirtuin 1 in Preventive or Therapeutic Options of Neurodegenerative Diseases. *Neuroscience*. 2022;504:79–92. doi:10.1016/j.neuroscience.2022.09.021
35. Zhou Y, Wang S, Li Y, Yu S, Zhao Y. SIRT1/PGC-1 $\alpha$  Signaling Promotes Mitochondrial Functional Recovery and Reduces Apoptosis after Intracerebral Hemorrhage in Rats. *Front Mol Neurosci*. 2017;10:443. doi:10.3389/fnmol.2017.00443
36. Lee YS, Choi JY, Mankhong S, et al. Sirtuin 1-dependent regulation of high mobility box 1 in hypoxia-reoxygenated brain microvascular endothelial cells: roles in neuronal amyloidogenesis. *Cell Death Dis*. 2020;11(12):1072. doi:10.1038/s41419-020-03293-0
37. Fang C, Xu H, Yuan L, et al. Natural Compounds for SIRT1-Mediated Oxidative Stress and Neuroinflammation in Stroke: a Potential Therapeutic Target in the Future. *Oxid Med Cell Longev*. 2022;2022:1949718. doi:10.1155/2022/1949718
38. Klotz LO, Sánchez-Ramos C, Prieto-Arroyo I, Urbánek P, Steinbrenner H, Monsalve M. Redox regulation of FoxO transcription factors. *Redox Biol*. 2015;6:51–72. doi:10.1016/j.redox.2015.06.019
39. Xing YQ, Li A, Yang Y, Li XX. The regulation of FOXO1 and its role in disease progression. *Life Sci*. 2018;193:124–131. doi:10.1016/j.lfs.2017.11.030
40. Rius-Pérez S, Torres-Cuevas I, Millán I, Ortega ÁL, Pérez S. PGC-1 $\alpha$ , Inflammation, and Oxidative Stress: an Integrative View in Metabolism. *Oxid Med Cell Longev*. 2020;2020:1452696. doi:10.1155/2020/1452696
41. Sivandzade F, Prasad S, Bhalerao A, Cucullo L. NRF2 and NF- $\kappa$ B interplay in cerebrovascular and neurodegenerative disorders: molecular mechanisms and possible therapeutic approaches. *Redox Biol*. 2019;21:101059. doi:10.1016/j.redox.2018.11.017
42. Singh V, Ubaid S. Role of Silent Information Regulator 1 (SIRT1) in Regulating Oxidative Stress and Inflammation. *Inflammation*. 2020;43(5):1589–1598. doi:10.1007/s10753-020-01242-9
43. Tossetta G, Fantone S, Montanari E, Marziani D, Goteri G. Role of NRF2 in Ovarian Cancer. *Antioxidants (Basel)*. 2022;11(4). doi:10.3390/antiox11040663
44. Gureev AP, Shaforostova EA, Popov VN. Regulation of Mitochondrial Biogenesis as a Way for Active Longevity: interaction Between the Nrf2 and PGC-1 $\alpha$  Signaling Pathways. *Front Genet*. 2019;10:435. doi:10.3389/fgene.2019.00435
45. Jena AB, Samal RR, Bhol NK, Duttaroy AK. Cellular Red-Ox system in health and disease: the latest update. *Biomed Pharmacother*. 2023;162:114606. doi:10.1016/j.biopha.2023.114606
46. Nolfi-Donagan D, Braganza A, Shiva S. Mitochondrial electron transport chain: oxidative phosphorylation, oxidant production, and methods of measurement. *Redox Biol*. 2020;37:101674. doi:10.1016/j.redox.2020.101674
47. Wang Y, Branicky R, Noë A, Hekimi S. Superoxide dismutases: dual roles in controlling ROS damage and regulating ROS signaling. *J Cell Biol*. 2018;217(6):1915–1928. doi:10.1083/jcb.201708007
48. Salihu AT, Muthuraju S, Idris Z, Izaini Ghani AR, Abdullah JM. Functional outcome after intracerebral haemorrhage - A review of the potential role of antiapoptotic agents. *Rev Neurosci*. 2016;27(3):317–327. doi:10.1515/revneuro-2015-0046
49. Ong A, Ramasamy TS. Role of Sirtuin1-p53 regulatory axis in aging, cancer and cellular reprogramming. *Ageing Res Rev*. 2018;43:64–80. doi:10.1016/j.arr.2018.02.004
50. Luo Q, Sun W, Wang YF, Li J, Li DW. Association of p53 with Neurodegeneration in Parkinson's Disease. *Parkinsons Dis*. 2022;2022:6600944. doi:10.1155/2022/6600944
51. Zhang Y, Khan S, Liu Y, et al. Modes of Brain Cell Death Following Intracerebral Hemorrhage. *Front Cell Neurosci*. 2022;16:799753. doi:10.3389/fncel.2022.799753
52. Yin JY, Lu XT, Hou ML, Cao T, Tian Z. Sirtuin1-p53: a potential axis for cancer therapy. *Biochem Pharmacol*. 2023;212:115543. doi:10.1016/j.bcp.2023.115543
53. Zhou J, Yang Z, Shen R, et al. Resveratrol Improves Mitochondrial Biogenesis Function and Activates PGC-1 $\alpha$  Pathway in a Preclinical Model of Early Brain Injury Following Subarachnoid Hemorrhage. *Front Mol Biosci*. 2021;8:620683. doi:10.3389/fmolb.2021.620683
54. Hees JT, Harbauer AB. Metabolic Regulation of Mitochondrial Protein Biogenesis from a Neuronal Perspective. *Biomolecules*. 2022;12(11):1595. doi:10.3390/biom12111595

## Drug Design, Development and Therapy

Dovepress

### Publish your work in this journal

Drug Design, Development and Therapy is an international, peer-reviewed open-access journal that spans the spectrum of drug design and development through to clinical applications. Clinical outcomes, patient safety, and programs for the development and effective, safe, and sustained use of medicines are a feature of the journal, which has also been accepted for indexing on PubMed Central. The manuscript management system is completely online and includes a very quick and fair peer-review system, which is all easy to use. Visit <http://www.dovepress.com/testimonials.php> to read real quotes from published authors.

Submit your manuscript here: <https://www.dovepress.com/drug-design-development-and-therapy-journal>